A Novel RFI Mitigation Method Using Source Rotation

Qiaolei Huang, *Student Member, IEEE*, Ling Zhang, *Student Member, IEEE*, Jagan Rajagopalan, Deepak Pai, Chen Chen, Amit Gaikwad, Chulsoon Hwang, *Senior Member, IEEE*, and Jun Fan, *Fellow, IEEE*

***Abstract*—This article proposes a novel radio frequency interference (RFI) mitigation method and applies it to a real consumer electronic device. Through near-field scanning, an equivalent dipole moment of the noise source containing the CPU and DDR memory chip is reconstructed. The near-field components of the victim Wi-Fi antenna are measured to obtain the transfer function. By determining the relationship between the dipole moment and the antenna near field, the noise source is rotated by a certain angle to reduce RFI. Rotating the source to reduce RFI is implemented in such a way that it does not compromise the signal integrity, and it does not require an additional shield can. New boards with the suggested changes are fabricated and the measured results show the RFI reduction up to 8 dB compared with the original board.**

***Index Terms*—Antenna, double data rate (DDR), dipole moment model, reciprocity, radio frequency interference (RFI), transfer function.**

I. Introduction

With the recent progress in the Internet of Things (IoT) and 5G technologies, billions of electronic devices in homes, factories, hospitals, cars, and many other places will be connected to the Internet [1]–[3]. These devices range from a refrigerator to a small car key fob, which are connected wirelessly to the Internet access point through Wi-Fi. Although the wireless technology in IoT devices provides great convenience, it also brings a lot of design challenges to RF integration engineers [4]–[6]. As the complexity of the digital subsystem increases, the potential noise sources in devices, such as a system on chip (SoC), high-speed traces, flexible cables, and power converters coupled to a colocated wireless antenna [7]–[12]. This unintended electromagnetic (EM) noise, called the RF interference (or simply RFI) interferes with the functionality of the wireless radio and reduces the usable wireless range of the device.

There are a few conventional ways to mitigate RFI. For example, the designers use absorbing materials, ferrite sheets, and shield cans to suppress noise radiation by modifying the coupling path [13]–[17]. However, in small form-factor products, sometimes it is difficult to apply a shield can or a layer of ferrite sheet due to the mechanical fabrication (product design) and cost limitations. Another approach is to modify the noise source itself. The clock or slew rate can be lowered to reduce the power spectral density of the noise source for frequencies where RFI issues occur. However, modifying the signal quality may reduce the signal integrity margin. The data encoding can also help to reduce RFI. A linear encoding technique that can reduce RFI by up to 14 dB is proposed in [16]. It is experimentally shown that an 8b/10b coding method can lead to the RFI reduction at 2.437 GHz in the range of 7–12 dB [17]. Another approach is to route the high-speed signals in a stripline instead of a microstrip. A stripline structure can provide better shielding compared with a microstrip structure. However, the choice of using a stripline routing or a microstrip routing can increase the printed circuit board (PCB) layer count, affect the signal integrity, and also add complexity to the overall board layout. Therefore, it is important to explore alternate ways to mitigate RFI without compromising signal integrity or adding cost to the product.

Recently, efficient methods to predict RFI in real products, such as laptops and cellphones, were introduced in [18]–[21]. A reciprocity theorem is used to estimate RFI by decomposing the overall RFI problem into two steps: forward problem and reverse problem. In the forward problem, the noise source's near-field radiation is studied, while the victim antenna is terminated. The forward problem can reconstruct the noise source into an equivalent dipole moment model. In the reverse problem, the antenna is excited and the noise source is turned OFF. Using the equivalent dipole moment and the reverse field, RFI from the noise source to the antenna can be obtained. However, there has been little effort to conduct a systematic way to mitigate RFI.

In this article, a popular consumer electronic device is studied. This small form-factor device has many complex digital subsystems, including CPU, double data rate (DDR) memory, power supply, and two Wi-Fi antennas (for the multiple-input and multiple-output (MIMO) functionality). Only the CPU, dynamic random-access memory (DRAM) ICs, and two Wi-Fi antennas are clearly shown in Fig. 1. The other parts are hidden to protect the intellectual property of the product. Through RFI measurements with and without the shielding, it is determined that the high-speed DDR3 traces on the main logic board are the dominant noise sources for RFI issues on the Wi-Fi antennas.

Manuscript received December 30, 2019; revised March 22, 2020; accepted May 13, 2020. This work was supported by the National Science Foundation under Grant IIP-1440110. *(Corresponding author: Jun Fan.)*

Qiaolei Huang, Ling Zhang, Chulsoon Hwang, and Jun Fan are with the Electromagnetic Compatibility Laboratory, Missouri University of Science and Technology, Rolla, MO 65409 USA (e-mail: qh5x4@mst.edu; lzd76@mst.edu; hwangc@mst.edu; jfan@mst.edu).

Jagan Rajagopalan, Deepak Pai, Chen Chen, and Amit Gaikwad are with the Wireless Technology Group of Amazon Lab126, Sunnyvale, CA 94089 USA (e-mail: rrajagop@amazon.com; hosadurg@amazon.com; cchc@amazon.com; gaikwada@amazon.com).

Color versions of one or more of the figures in this article are available online at https://ieeexplore.ieee.org.

Digital Object Identifier 10.1109/TEMC.2020.2995828

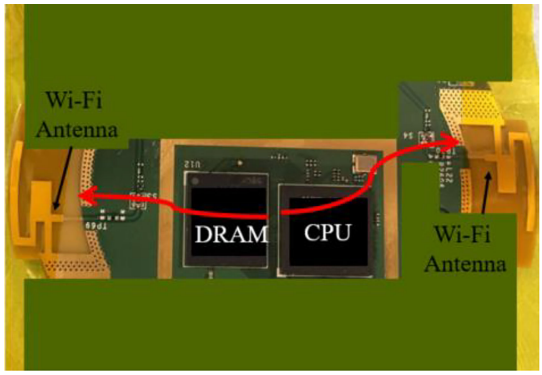

Fig. 1. DUT illustration. DDR noise source couples to nearby Wi-Fi antennas.

Having identified the noise, the steps outlined in the following are followed to measure, reconstruct, and mitigate the RFI issue.

First, the near-field measurements of source and antenna are performed using an EM scanner to understand the RFI radiation and coupling physics. Then, the dipole moment based reciprocity method is utilized to propose the RFI mitigation methods, such as the movement and/or rotation of noise source. The theoretical derivations and steps to maximize the RFI reductions for two antennas are also provided. Finally, the results of the final modified board with the reduced RFI are presented. The comparisons of the measured RFI reduction and the theoretical RFI reduction for both antennas are also presented.

II. Noise Source and Antenna Characterization

An EM scanner with a spectrum analyzer is a fast and convenient tool to measure near-field emissions from any radiating source. Using an EM scanner, the near-field distribution of noise sources (i.e., SoC and DDR3 interface) is measured. The measurement setup and a simple illustration are shown in Fig. 2. During the measurement, the device was configured in a stress mode to emulate a high-speed data transfer between the CPU and DDR memory chip. The resonant-type *H*-field probe at 2.45 GHz is used and the scanning is performed at channel 6 of 2.4 GHz Wi-Fi. The resolution bandwidth of the spectrum analyzer is set to 100 kHz with a sweep time of 50 ms. An average detector is used, and the scan data are sampled using a max hold mode for 15 s. Furthermore, the scanning area was chosen to be 30 × 30 mm with a 2 mm step.

The measured near-field patterns with H_x and H_y components are shown in Fig. 3(a). The *H*-field patterns are similar to the field patterns of a single magnetic dipole M_y. Similar field patterns were observed in measurements of some cellphones and laptops [18]. According to the article presented in [18], a few other projects also use only one single magnetic dipole moment to replace the noise source based on its *H*-field patterns. Once the source dipole is identified as one single magnetic dipole moment, the magnitude of the magnetic dipole can be calculated using the least squares method with the magnitude-only data, as used in [19] and [20]. Fig. 3(b) shows the near-field patterns calculated from the reconstructed magnetic dipole. According to EMs theory and analysis in [21], the pattern center is the location of the dipole moment. In the measured field patterns, the

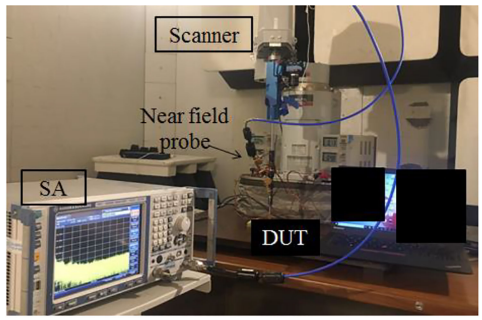

(a)

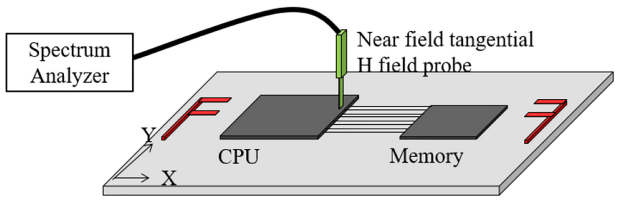

(b)

Fig. 2. Near-field scanning measurement setup of the tangential *H*-field above the DUT. (a) Real picture. (b) Simple illustration. The measurement loop in the tangential *H*-field probe was placed facing the *X* and *Y* directions to measure H_x and H_y separately.

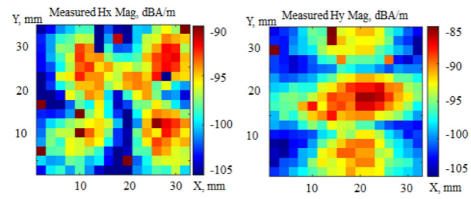

(a)

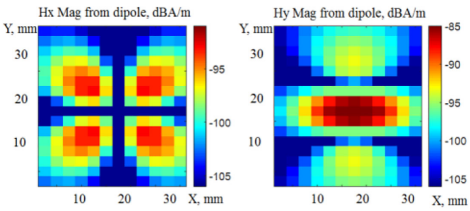

(b)

Fig. 3. (a) Measured $|H_x|$ and $|H_y|$. (b) Calculated $|H_x|$ and $|H_y|$ from the reconstructed magnetic dipole.

pattern center corresponds to the center of the microstrip lines, as depicted in Fig. 4. The reconstructed magnetic dipole M_y can be understood as an electric current loop in the *xz*-plane facing the *Y*-direction. Although the field patterns in this device are similar to those in [21], it is worthwhile to point out that the underlying physics behind the dipole moment of these two products is different. The magnetic dipole moment in this product is caused by the microstrip, as shown in Fig. 4. However, the magnetic dipole moment in [21] is caused by the transition parts from the embedded stripline to the ICs.

Since the radiation source is a single M_y dipole moment in the forward problem, according to the article presented in [18], the coupled voltage to the victim antenna can be calculated by

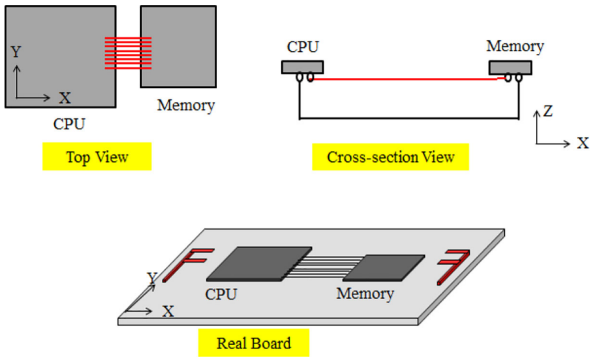

Fig. 4. Routing between the CPU and memory IC.

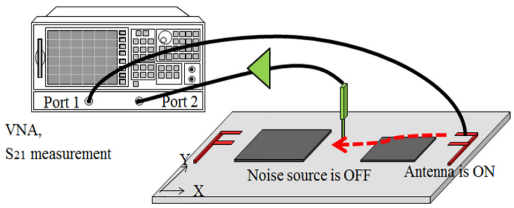

Fig. 5. Measurement setup of the reverse problem with the antenna excited. The measurement loop in the tangential *H*-field probe was placed facing the *X* and *Y* directions to measure H_x and H_y separately in the reverse problem.

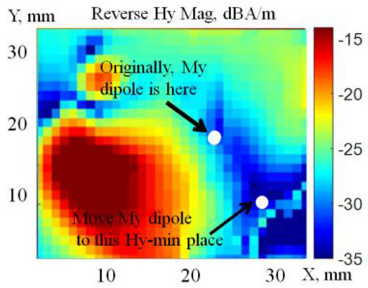

Fig. 6. Measured $|H_y|$ in the reverse problem when the victim antenna radiates. Moving the M_y dipole to the smallest H_y place reduces the noise coupling and alleviates the RF desense issue.

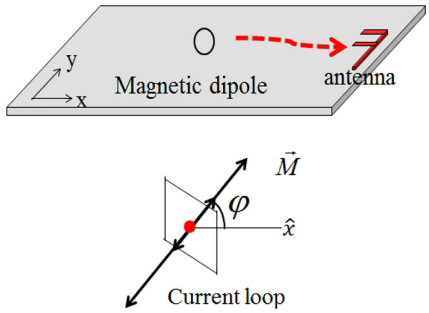

Fig. 7. Simple diagram of the rotation problem.

the following equation:

$$U_{\text{fwd}} = \frac{Z_L}{2U_{\text{rev}}^{+}} \left[\vec{H}_{\text{rev}} \cdot \vec{M}_{\text{fwd}} \right] \tag{1}$$

where U_{fwd} is the coupled voltage at the antenna port due to the noise source, M_{fwd} is the dipole moment in the forward problem (M_y in this device), Z_L is the load impedance (50 Ω), U_{rev}^{+} is the incident voltage from the antenna port in the reverse problem, and H_{rev} is the *H*-field in the reverse problem with the incident voltage of U_{rev}^{+}.

The measurement setup of the reverse problem is shown in Fig. 5. A vector network analyzer (VNA) is used along with the EM scanner instead of the spectrum analyzer. The victim antenna is excited using port 1. Port 2 of the VNA is connected to the near-field probe of the EM scanner. With the noise source turned OFF, the near-field components of the antenna are measured by capturing S_{21} from VNA. Using the probe calibration factor, the *H*-field at the location of the dipole moment can be obtained. The measured $|H_y|$ in the reverse problem is shown in Fig. 6. In the scanning plane, it is observed there are hot spots and cold spots of the antenna *H*-field. According to (1), smaller H_y can lead to smaller coupled voltage on the antenna port. Thus, moving the M_y dipole (the noise source) to the smallest H_y location can help in reducing the RFI. However, in this device, the smallest H_y location is at the edge of the scanning plane, which is also the edge of the main logic board. If this change was applied, CPU and memory ICs would have to be placed at the edge of the board, which is not a practical layout change. Reducing the magnitude of equivalent dipole moment M_y can also lead to a smaller RFI. Since the magnetic dipole moment is essentially an electric current loop, either the current on the loop or the loop area can be reduced. Although both options can successfully reduce RFI, they also impact the signal integrity as mentioned above; thus, these are not the main focus of this article.

III. RFI Reduction by Rotating Noise Source

In (1), it is worth noting that there is an inner product between the two vectors: the noise source and the reverse field (i.e., $\vec{H}_{\text{rev}}$ and $\vec{M}_{\text{fwd}}$). In this work, a novel method in manipulating the angle difference of the two vectors is undertaken. With a certain angle, the inner product of these two vectors can be minimized. A general expression of $\vec{H}_{\text{rev}}$ and $\vec{M}_{\text{fwd}}$ is given as follows:

$$\begin{aligned} \vec{H}_{\text{rev}} &= \hat{x}|H_x|e^{i\theta_x} + \hat{y}|H_y|e^{i\theta_y} + \hat{z}|H_z|e^{i\theta_z} \\ \vec{M}_{\text{fwd}} &= \hat{x}|M|e^{i\theta_m}\cos\varphi + \hat{y}|M|e^{i\theta_m}\sin\varphi \end{aligned} \tag{2}$$

where $\hat{x}$, $\hat{y}$, and $\hat{z}$ are the unit vectors along the *x*-, *y*-, and *z*-axis, respectively. $|H_x|$ and θ_x are the magnitude and phase of the complex number H_x, which can be measured in the reverse problem. Similar definitions apply for H_y and H_z. $|M|$ and θ_m are the magnitude and phase of the original *M* dipole, respectively. φ is the rotation angle, relative to the *x*-axis. The rotation of the magnetic dipole moment corresponds to the different routing angles of the noise traces or the different angle placement of noise IC in real-world applications. If the magnetic dipole is rotated to a certain angle in the *xy*-plane, the magnetic dipole moment will have both *x* and *y* components. Fig. 7 shows a simple diagram of the rotation problem. Substituting (2) into (1), and assuming $U_{\text{rev}}^{+} = 1$ V and $Z_L = 50\ \Omega$, the coupled voltage

can be obtained as follows:

$$\begin{aligned} U_{\text{fwd}} &= 25\vec{H}_{\text{rev}} \cdot \vec{M}_{\text{fwd}} \\ &= 25(\hat{x}|H_x|e^{i\theta_x} + \hat{y}|H_y|e^{i\theta_y} + \hat{z}|H_z|e^{i\theta_z}) \\ &\cdot (\hat{x}|M|e^{i\theta_m}\cos\varphi + \hat{y}|M|e^{i\theta_m}\sin\varphi) \\ &= 25|M|e^{i\theta_m}(|H_x|e^{i\theta_x}\cos\varphi + |H_y|e^{i\theta_y}\sin\varphi) \end{aligned} \quad (3)$$

where $|M_\varphi|$ is the magnitude of the magnetic dipole after rotation angle φ in the *xy*-plane; and $|M_\varphi|$ remains the same value $|M|$ for any rotation angle φ in the *xy*-plane. U_{fwd} is a complex number. $|U_{\text{fwd}}|$ can be obtained from the real part and the imaginary part of the complex number (4) shown at the bottom of this page, where $|H_\varphi|$ is the *H*-field component along $\vec{M}_{\text{fwd}}$, which is the perpendicular direction over the current loop. A special case for this rotation problem is that the reverse *H*-field is linearly polarized. Namely, the phase difference between H_x and H_y fulfills the relationship such that $\theta_x - \theta_y = \pm n\pi$, where *n* is an integer. Then, it leads to $\cos\theta_x\cos\theta_y + \sin\theta_x\sin\theta_y = \pm 1$. In this special case, (4) is simplified as

$$\begin{aligned} |U_{\text{fwd}}| &= 25|M|(|H_x|\cos\varphi \pm |H_y|\sin\varphi) \\ |U_{\text{fwd}}| &= 25|M_\varphi||H_\varphi| \\ |H_\varphi| &= (|H_x|\cos\varphi \pm |H_y|\sin\varphi) \\ &= (\hat{x}|H_x| \pm \hat{y}|H_y|)\cdot(\hat{x}\cos\varphi + \hat{y}\sin\varphi). \end{aligned} \quad (5)$$

In (5), $|H_\varphi|$ is actually an inner product of two vectors, both of which are real numbers. For an inner product of two real value vectors in the *xy*-plane, there is always a zero case when two vectors are perpendicular to each other as the rotation angle φ is a variable here. In contrast, (1) is also an inner product of two vectors, both of which, however, are complex numbers. In (1), there is no guarantee that the inner product can achieve zero. Equation (1) depicts a general case ($\theta_x - \theta_y \neq \pm n\pi$), while (5) shows the special case ($\theta_x - \theta_y = \pm n\pi$). A simple diagram is drawn in Fig. 8 to illustrate the special case ($\theta_x - \theta_y = \pm n\pi$). In Fig. 8, when the current loop is placed along the reverse *H*-field line, there are no *H*-field lines penetrating through the current loop. Thus, the inner product between the *H*-field vector and the normal vector of the loop is zero and no noise coupling occurs. The worst RFI for the linearly polarized case happens when the *H*-field vector is perpendicular to the current loop. Another diagram is drawn in Fig. 9 to illustrate the general case ($\theta_x - \theta_y \neq \pm n\pi$). In the general case, the reverse *H*-field is elliptically polarized. In Fig. 9, when the loop is placed along the longer axis of the ellipse, there are less *H*-field lines penetrating through the current loop. Thus, the inner product between the *H*-field vector and the normal vector of the loop becomes the minimum. The worst RFI for the elliptically polarized case happens when the *H*-field vector is placed along the shorter axis. There are more *H*-field lines penetrating through the current loop. Thus, the inner product between the *H*-field vector and the normal direction of the loop becomes the maximum.

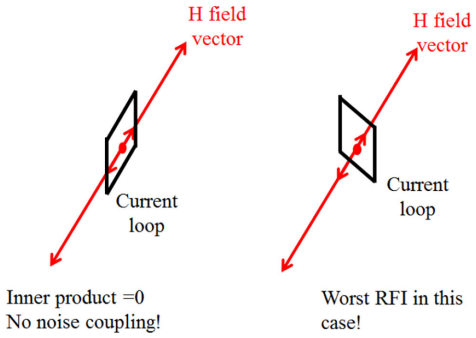

Fig. 8. Special case for the rotation problem: Reverse *H*-field is linearly polarized ($\theta_x - \theta_y = \pm n\pi$).

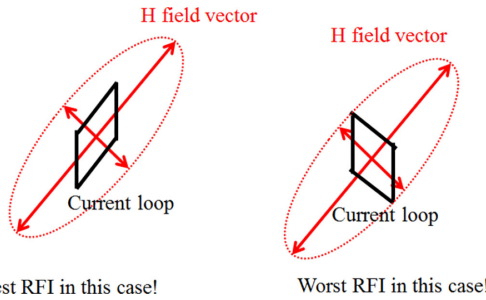

Fig. 9. General case for the rotation problem: Reverse *H*-field is elliptically polarized ($\theta_x - \theta_y \neq \pm n\pi$).

Taking one of the Wi-Fi antennas on this board for analysis (right-side antenna), the magnitude and phase of reverse H_x and H_y are obtained from the reserve problem measurement, as shown in Fig. 5. The measured phase difference of reverse H_x and H_y is 181°, which is very close to the special case in Fig. 8 (reverse *H*-field has the phase difference of 180° or 0°). It is expected that RFI will be minimum at a certain rotation angle φ. By substituting the magnitude and phase of reverse H_x and H_y into (4), the coupled voltage at any rotation angle φ is obtained. The theoretical RFI reduction is defined by subtracting the coupled voltage at any rotation angle φ from the original coupled voltage, where the dipole moment is M_y (where φ is 90°).

As stated above, $|M_\varphi|$ stays the same for any rotation angle φ in the *xy*-plane. The RFI reduction is indeed from the reduction in $|H_\varphi|$ compared with the original $|H_y|$ (namely $\varphi = 90°$).

$$\begin{aligned} |U_{\text{fwd}}| &= 25|M|\sqrt{(|H_x|^2\cos^2\varphi + |H_y|^2\sin^2\varphi + 2|H_x||H_y|\sin\varphi\cos\varphi(\cos\theta_x\cos\theta_y + \sin\theta_x\sin\theta_y)} \\ |U_{\text{fwd}}| &= 25|M||H_\varphi| \\ |H_\varphi| &= \sqrt{(|H_x|^2\cos^2\varphi + |H_y|^2\sin^2\varphi + 2|H_x||H_y|\sin\varphi\cos\varphi(\cos\theta_x\cos\theta_y + \sin\theta_x\sin\theta_y)} \end{aligned} \quad (4)$$

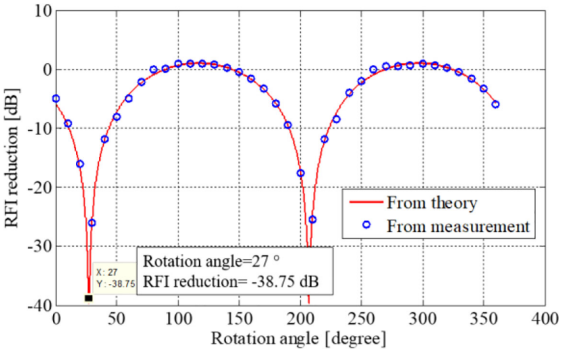

Fig. 10. Theoretical and measured RFI reduction for various rotation angle φ. The noise source is kept at the same place. When the rotation angle is 27°, the RFI will reduce 38.75 dB compared with the original case.

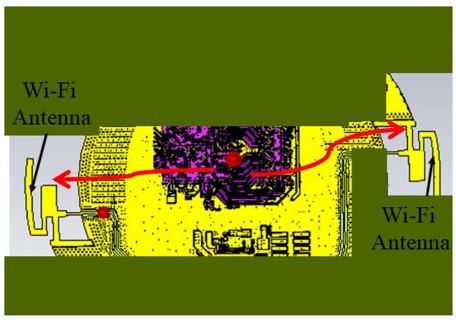

Fig. 11. Simulation model containing the PCB, victim antennas, and the equivalent dipole moment (current loop in this case).

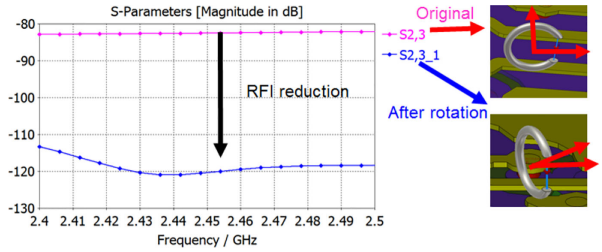

Fig. 12. RFI reduction in the simulation between $\varphi = 90°$ (original case) and $\varphi = 27°$ (best rotation angle).

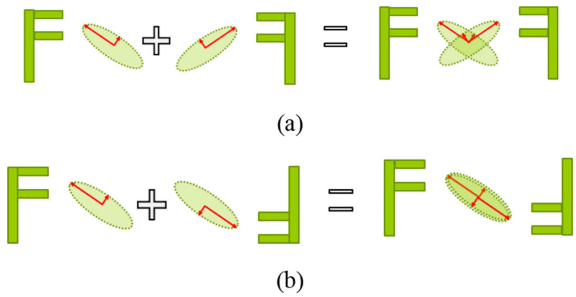

Fig. 13. RFI reduction diagram for two antennas. (a) Both antennas are symmetrical over the *y*-axis. (b) Both antennas are symmetrical over the dipole moment source point.

The measurement is also done to show the reduction in $|H_\varphi|$ using the setup, as shown in Fig. 5. The baseline was set as the measured $|H_y|$ when the probe is facing the *Y*-direction. For any other rotation angle φ, the probe will be rotated to measure $|H_\varphi|$. The measured reduction in $|H_\varphi|$ is defined by subtracting $|H_\varphi|$ at any rotation angle φ from the original $|H_y|$.

In Fig. 10, RFI reduction from the measurement is compared with the theoretical value calculated from (4) for any rotation angle φ. Good agreement seen between the measurement and the theory validates the proposed methodology. When the rotation angle is 27°, the maximum RFI reduction is achieved to be 38.75 dB. Simulations are also done to validate the proposed rotation methodology. In the simulation model, as shown in Fig. 11, the actual noise source ICs and traces are replaced by a single magnetic dipole moment, which is actually a current loop in the simulation. The construction of the current loop is the same as the article presented in [22]. All the other PCBs and victim antennas are kept the same. In the simulation, the RFI between the original case and the $\varphi = 27°$ rotation case is compared. The simulation results are shown in Fig. 12. The simulated RFI reduction between the original case and the $\varphi = 27°$ rotation case is 38 dB, which agrees very well with the measured and theoretical RFI reduction.

IV. RFI Reduction for Two Antennas

In the previous sections, a theoretical way to improve RFI without impacting the signal integrity and adding cost to the product is introduced. Simulations and measurements show that rotating the magnetic dipole moment, which is the noise source, to $\varphi = 27°$ can significantly reduce RFI for one of the selected Wi-Fi antennas on this device (the right-side antenna). However, in an actual device, RFI on the two antennas (for MIMO functionality) needs to be improved together. Two special cases are studied for the two-antenna system.

The first special case is that the two antennas are symmetrical around the *y*-axis. The second special case is that the two antennas are symmetrical to the source point of the magnetic dipole moment. Let us assume that the near field is a general case, i.e., elliptically polarized. Then, for the *y*-symmetry case in Fig. 13(a), the best angles for the RFI reduction are achieved at different angles, as denoted by the two different shorter axes of the two ellipses. In other words, there is no best angle to achieve the maximum RFI reduction for both antennas. In contrast, for the point-symmetry case in Fig. 13(b), the best angles for the RFI reduction on both antennas are achieved along the same line, as denoted by the shorter axes of the same ellipse. For the first special case in Fig. 13(a), where two antennas are symmetrical around the *y*-axis, the theoretical RFI reduction can be calculated by taking the simulated magnitude and phase of H_x and H_y of both antennas into (4). The theoretical RFI reductions for both antennas are shown in Fig. 14(a). The best angle to achieve the maximum RFI reduction for the right-side antenna and the left-side antenna is $\varphi = 27°$ and $\varphi = 153°$, respectively. In this *y*-symmetry case, there is no best angle to achieve the maximum RFI reduction for both antennas. On the contrary, for the point-symmetry case in Fig. 13(b), there is a best angle $\varphi = 27°$ to achieve the maximum RFI reductions for both antennas, as shown in Fig. 14(b).

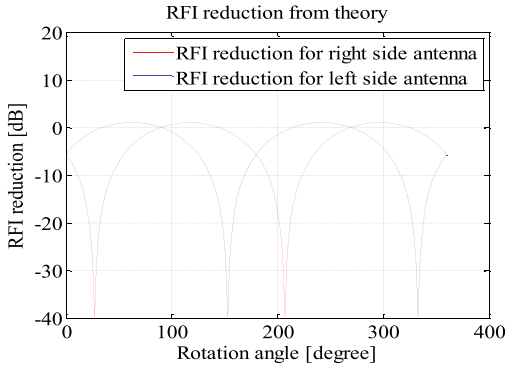

(a)

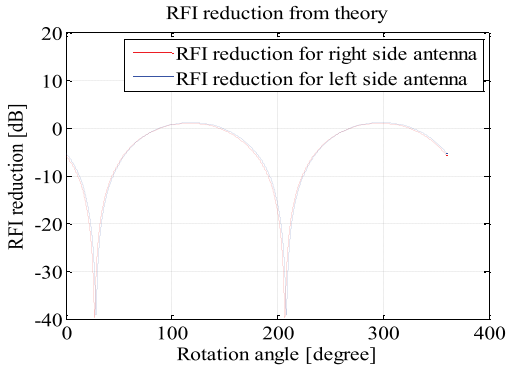

(b)

Fig. 14. Theoretical RFI reduction at any rotation angle φ for two antennas. (a) Both antennas are symmetrical over the *Y*-axis. (b) Both antennas are symmetrical over the dipole moment source point.

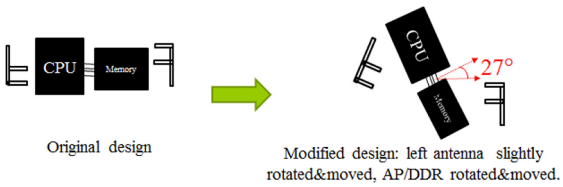

Fig. 15. Original design and the modified design ($\varphi = 27°$).

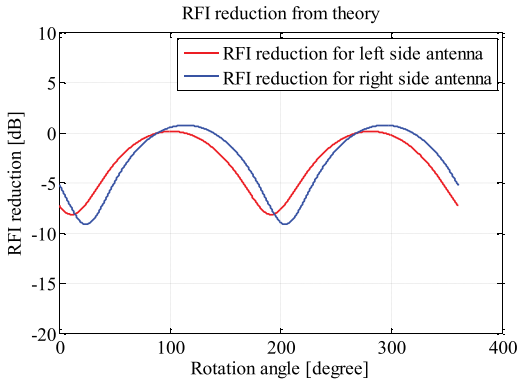

Fig. 16. Theoretical RFI reduction at any rotation angle φ for the two antennas on the modified board.

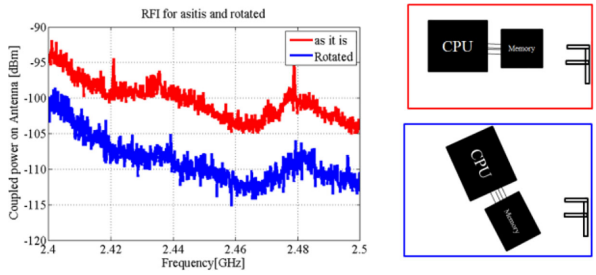

Fig. 17. Measured RFI reduction for the right-side antenna between the original design and the modified design ($\varphi = 27°$). RFI reduction for the right-side antenna is 8 dB at 2.437 GHz.

TABLE I
PREDICTED AND MEASURED RFI REDUCTIONS FOR TWO ANTENNAS ON THE MODIFIED BOARD WITH $\varphi = 27°$

f=2.437GHz	Predicted RFI reduction	Measured RFI reduction	Error
Left-side Antenna	6.5 dB	4 dB	2.5dB
Right-side Antenna	9 dB	8 dB	1 dB

However, due to the limitation of the layout space on this board, it was difficult to rotate the dipole moment to $\varphi = 27°$ while keeping the dipole location the same and also keeping two-antenna points symmetrical over the dipole moment source. So, the ideal case in Fig. 14(b) was not feasible in the real board design. In the final modified layout, the locations of the noise source were moved up 3 mm, in order to accommodate the placement of the other components. Because of the movement of 3 mm, for the right-side antenna, the phase difference of reverse H_x and H_y at the new location is 153°, which is worse than the almost linearly polarized case in the original location (originally, the phase difference of reverse H_x and H_y is 181°). It is expected that the RFI reduction in this new location will not be as good as 38 dB for the original location (181° as the phase difference). Fig. 15 shows the comparisons between the original board and the final modification board. Based on the simulated reverse-field distribution of two antennas, the theoretical RFI reduction for any rotation angle φ is shown in Fig. 16. When the rotation angle φ is 27°, the theoretical RFI reduction for the left- and right-side antennas is 6.5 and 9 dB. It is a compromise to achieve good RFI reductions on both antennas and also take care of other component placements.

The device with the new placement has been fabricated and measured. The measured RFI for the right-side antenna between the modified design and the original design is shown in Fig. 17. The measured RFI reduction for the left-side antenna is 4 dB and for the right-side antenna is 8 dB at 2.437 GHz (channel 6 of 2.4 GHz Wi-Fi). The RFI reductions for both antennas agree well with the theoretical RFI reduction. The error is within 2.5 dB, as listed in Table I.

Fig. 18(a) shows the real picture of the modified board, as illustrated in Fig 15, which is simply called the "SR27" board due to the rotation angle $\varphi = 27°$. On the "SR27" board, good

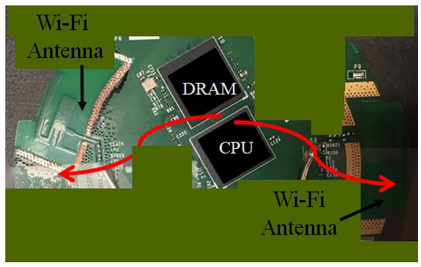

(a)

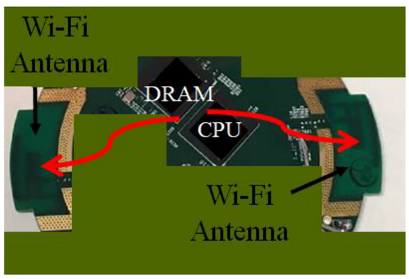

(b)

Fig. 18. (a) Real picture of the modified board, as illustrated in Fig 15, which is simply called the "SR27" board. (b) Real picture of the modified board for the rotation angle as 45°, which is simply called the "SR45" board.

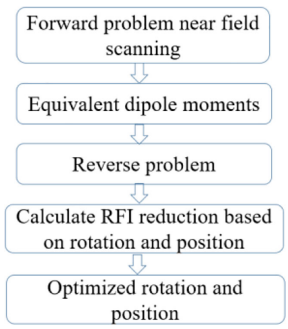

Fig. 19. Workflow for the RFI mitigation using the proposed method.

RFI reductions are achieved for both antennas. To add another data point in this research, another modified board with the rotation angle as 45° (simply called the "SR45" board) was also manufactured. The real picture of the "SR45" board is shown in Fig. 18(b). For the "SR45" board, the measured RFI reduction for the left-side antenna is 1 dB and for the right-side antenna is 4 dB at 2.437 GHz. By comparison, the theoretical RFI reduction on the "SR45" board for the left-side antenna is 3 dB and for the right-side antenna is 7.5 dB at 2.437 GHz. The error between the measurement and theory is within 3.5 dB.

Overall, the modified "SR27" board provides more RFI reductions than the "SR45" board. The theory can agree with measurements. The proposed RFI reduction methodology is validated successfully. The workflow of using the proposed method to achieve RFI mitigation is shown in Fig. 19. It is also worthwhile to mention that this article mainly focuses on the rotation of the radiation source but not on the antennas due to the shape of the product. For other products, the antennas can also be rotated and repositioned to minimize RFI, as shown in [23].

V. Summary

In this article, the RFI reduction for a real consumer electronic device is studied. Considering the layout limitation of the product, the proposed RFI mitigation involves rotating the CPU and DDR chip by a certain angle without compromising signal integrity. In addition to retaining signal integrity, the proposed method does not require a shield can to meet RFI specification for achieving the desired Wi-Fi performance. New boards with the suggested changes were manufactured, and the measured results showed the RFI reduction up to 8 dB compared with the original board. The measured RFI reduction has good agreement with the theoretical RFI reduction. The proposed method enables a new dimension to the RFI mitigation with cost-saving opportunities.

References

[1] P. Shen, Y. Qi, W. Yu, J. Fan, and F. Li, "OTA measurement for IoT wireless device performance evaluation: Challenges and solutions," *IEEE Internet Things J.*, vol. 6, no. 1, pp. 1223–1237, Feb. 2019.

[2] D. Zhang, Z. Zhou, S. Mumtaz, J. Rodriguez, and T. Sato, "One integrated energy efficiency proposal for 5G IoT communications, " *IEEE Internet Things J.*, vol. 3, no. 6, pp. 1346–1354, Dec. 2016.

[3] P. Shen, Y. Qi, W. Yu, J. L. Drewniak, M. Yu, and F. Li, "An RTS-based near-field MIMO measurement solution—A step toward 5G," *IEEE Trans. Microw. Theory Techn.*, vol. 67, no. 7, pp. 2884–2893, Jul. 2019.

[4] Y.-F. Shu, X.-C. Wei, J. Fan, R. Yang, and Y.-B. Yang, "An equivalent dipole model hybrid with artificial neural network for electromagnetic interference prediction," *IEEE Trans. Microw. Theory Techn.*, vol. 67, no. 5, pp. 1790–1797, May 2019.

[5] W.-J. Zhao, E.-X. Liu, B. Wang, S.-P. Gao, and C. E. Png, "Differential evolutionary optimization of an equivalent dipole model for electromagnetic emission analysis," *IEEE Trans. Electromagn. Compat.*, vol. 60, no. 6, pp. 1635–1639, Dec. 2018.

[6] Y. Wang, S. Wu, J. Zhang, Z. Yang, K. Wu, and J. Fan, "A simulation-based coupling path characterization to facilitate desense design and debugging," in *Proc. IEEE Symp. Electromagn. Compat., Signal Integrity Power Integrity*, 2018, pp. 150–155.

[7] Q. Huang, F. Zhang, T. Enomoto, J. Maeshima, K. Araki, and C. Hwang, "Physics-based dipole moment source reconstruction for RFI on a practical cellphone," *IEEE Trans. Electromagn. Compat.*, vol. 59, no. 6, pp. 1693–1700, Dec. 2017.

[8] S. Shinde *et al.*, "Investigation of interference in a mobile phone from a DC-to-DC converter," in *Proc. IEEE Int. Symp. Electromagn. Compat.*, 2013, pp. 616–620.

[9] C. Hwang *et al.*, "Noise coupling path analysis for RF interference caused by LCD noise modulation," in *Proc. IEEE Int. Symp. Electromagn. Compat.*, 2016, pp. 348–352.

[10] Y. Sun, B.-C. Tseng, H. Lin, and C. Hwang, "RFI noise source quantification based on reciprocity," in *Proc. IEEE Symp. Electromagn. Compat., Signal Integrity Power Integrity*, 2018, pp. 548–553.

[11] H. H. Park, J. H. Kwon, S. I. Kwak, and S. Ahn, "Electromagnetic shielding analysis of multiple slits on a metal plate coated with a ferrite sheet," *IEEE Trans. Electromagn. Compat.*, vol. 58, no. 5, pp. 1448–1455, Oct. 2016.

[12] C. Wu *et al.*, "Estimating the near field coupling from SMPS circuits to a nearby antenna using dipole moments," in *Proc. IEEE Int. Symp. Electromagn. Compat.*, 2016, pp. 353–357.

[13] H. H. Park, "Reduction of electromagnetic noise coupling to antennas in metal-framed smartphones using ferrite sheets and multi-via EBG structures," *IEEE Trans. Electromagn. Compat.*, vol. 60, no. 2, pp. 394–401, Apr. 2018.

[14] V. Rathi and V. Panwar, "Electromagnetic interference shielding analysis of conducting composites in near- and far-field region," *IEEE Trans. Electromagn. Compat.*, vol. 60, no. 6, pp. 1795–1801, Dec. 2018.

[15] Y. Ku, H. H. Park, and C. Hwang, "Zero-height and broadband magnetic dipole source generation for board level shield can evaluation," *IEEE Trans. Electromagn. Compat.*, vol. 61, no. 6, pp. 1860–1866, Dec. 2019.

[16] E. X. Alban, S. Sajuyigbe, H. Skinner, A. Alcocer, and R. Camacho, "Mitigation techniques for RFI due to broadband noise," in *Proc. IEEE Int. Symp. Electromagn. Compat.*, 2014, pp. 159–164.

[17] C.-C. Chou and T.-L. Wu, "EMI-reduction coding based on 8b/10b," in *Proc. IEEE Int. Symp. Electromagn. Compat. Signal/Power Integrity*, 2017, pp. 373–376.
[18] Q. Huang, T. Enomoto, S. Seto, K. Araki, J. Fan, and C. Hwang, "A transfer function based calculation method for radio frequency interference," *IEEE Trans. Electromagn. Compat.*, vol. 61, no. 4, pp. 1280–1288, Aug. 2019.
[19] Y. Sun, H. Lin, B.-C. Tseng, D. Pommerenke, and C. Hwang, "Mechanism and validation of USB 3.0 connector caused radio frequency interference," *IEEE Trans. Electromagn. Compat.*, to be published, doi: 10.1109/TEMC.2019.2925935.
[20] Q. Huang and J. Fan, "Machine learning based source reconstruction for RF desense," *IEEE Trans. Electromagn. Compat.*, vol. 60, no. 6, pp. 1640–1647, Dec. 2018.
[21] Q. Huang *et al.*, "Desense prediction and mitigation from DDR noise source," in *Proc. IEEE Symp. Electromagn. Compat. Signal Integrity Power Integrity*, 2018, pp. 139–144.
[22] Q. Huang, Y. Liu, L. Li, Y. Wang, C. Wu, and J. Fan, "Radio frequency interference estimation using transfer function based dipole moment model," in *Proc. IEEE Asia-Pac. Symp. Electromagn. Compat.*, 2018, pp. 115–120.
[23] D. Pai, J. Rajagoplan, A. Mohan, and Q. Huang, "Optimized wireless system design with minimal RFI using antenna near field approach," in *Proc. DesignCon*, Jan. 2020.

Qiaolei Huang (Student Member, IEEE) received the B.E. degree in electrical and computer engineering from the Huazhong University of Science and Technology, Wuhan, China, in 2013, and the M.S. degree in electrical engineering, in 2016 from Electromagnetic Compatibility (EMC) Laboratory, Missouri University of Science and Technology, Rolla, MO, USA, where he is currently working toward the Ph.D. degree in electrical engineering.

His research interests include radio frequency interference, radiated emission modeling, and EMC measurement method.

Mr. Huang was the recipient of the best papers of DesignCon 2018, DesignCon 2019, and 2018 Joint IEEE EMC and APEMC Symposium.

Ling Zhang (Student Member, IEEE) received the B.S. degree in electrical engineering from the Huazhong University of Science and Technology, Wuhan, China, in June 2015, and the M.S. degree in electrical engineering, in December 2017 from the Missouri University of Science and Technology, Rolla, MO, USA, where he is currently working toward the Ph.D. degree in electrical engineering with Electromagnetic Compatibility Laboratory.

From 2016 to 2017, he was a student intern with Cisco. His research interests include machine learning applications in PI/SI/EMC, RFI source reconstruction and coupling paths analysis, and the emission source microscopy technique for the EMI source localization.

Jagan Rajagopalan received the master's degree with focus on wireless technology from the University of South Florida, Tampa, FL, USA, in 2010.

He is a Senior RF System Engineer in Wireless Technology Group, Amazon Lab126, Sunnyvale, CA, USA, where he is currently an Engineering Leader. He has 10+ years of work experience in consumer electronics industry. He is the author of multiple IEEE conference papers and holds multiple U.S. patents in the field of defense, EMI, and RF system design.

Deepak Pai received the master's degree in electrical engineering from the University of Texas at Dallas, Richardson, TX, USA, in 2014.

He is a Wireless Systems Engineer with Wireless Technology Group, Amazon Lab126, Sunnyvale, CA, USA, where he is currently an RF System/EM Engineer. He has five years of work experience in the consumer electronics industry. He is the author of multiple IEEE conference papers and holds multiple U.S. patents in the field of EM and antenna design.

Chen Chen received the Ph.D. degree in electrical engineering from Virginia Tech, in 2007.

He is a Wireless Design Manager with Wireless Technology Group, Amazon Lab126, Sunnyvale, CA, USA. He has published more than 10 journal papers and book chapters, as well as more than 30 conference papers. He received Young Scientist Award from URSI in 2008 and was elected as Session Chairs of multiple IEEE conferences.

Amit Gaikwad received the M.S. degree in electrical engineering from New York University, in 2007.

He is a Senior Wireless Design Manager with Wireless Technology Group, Amazon Lab126, Sunnyvale, CA, USA.

Chulsoon Hwang (Senior Member, IEEE) received the B.S., M.S., and Ph.D. degrees in electrical engineering from the Korea Advanced Institute of Science and Technology, Daejeon, South Korea, in 2007, 2009, and 2012, respectively.

From 2012 to 2015, he was a Senior Engineer with the Global Technology Center, Samsung Electronics, Suwon, South Korea, where he was mainly engaged in the radio frequency interference design for mobile phones. In July 2015, he joined the Missouri University of Science and Technology (formerly University of Missouri-Rolla), Rolla, MO, USA, where he is currently an Assistant Professor with the Electromagnetic Compatibility Laboratory. His current research interests include the signal/power integrity in high-speed digital systems, inter/intra EMC, and 3-D IC integrations.

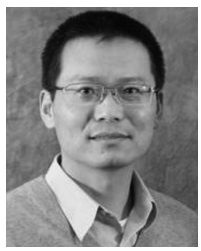

Jun Fan (Fellow, IEEE) received the B.S. and M.S. degrees from Tsinghua University, Beijing, China, and the Ph.D. degree from the Missouri University of Science and Technology (Missouri S&T), Rolla, MO, USA, in 1994, 1997, and 2000, respectively, all in electrical engineering.

From 2000 to 2007, he was a Consultant Engineer with NCR Corporation, San Diego, CA, USA. In July 2007, he joined the Missouri S&T, where he is currently a Professor and a Director of the Electromagnetic Compatibility Laboratory. He also serves as the Director of the National Science Foundation Industry/University Cooperative Research Center for Electromagnetic Compatibility and a Senior Investigator of Missouri S&T Material Research Center. His research interests include signal integrity and EMI designs in high-speed digital systems, dc power-bus modeling, intrasystem EMI and RF interference, PCB noise reduction, differential signaling, and cable/connector designs.

Dr. Fan was the recipient of IEEE EMC Society Technical Achievement Award, in August 2009. He is currently an Associate Editor for the IEEE TRANSACTIONS ON ELECTROMAGNETIC COMPATIBILITY and the IEEE *EMC Magazine*.